Behavioral/Systems/Cognitive

Malfunction of Respiratory-Related Neuronal Activity in Na^+, K^+-ATPase α2 Subunit-Deficient Mice Is Attributable to Abnormal Cl^- Homeostasis in Brainstem Neurons

Keiko Ikeda,[1] Hiroshi Onimaru,[3] Junko Yamada,[4] Koichi Inoue,[5] Shinya Ueno,[5] Tatsushi Onaka,[2] Hiroki Toyoda,[1] Akiko Arata,[6] Tomo-o Ishikawa,[7,8] Makoto M. Taketo,[7,8] Atsuo Fukuda,[4,5] and Kiyoshi Kawakami[1]

[1]Division of Biology, Center for Molecular Medicine, and [2]Department of Physiology, Jichi Medical School, Kawachi, Tochigi 329-0498, Japan, [3]Department of Physiology, Showa University School of Medicine, Shinagawa-ku, Tokyo 142-8555, Japan, [4]Department of Biological Information Processing, Graduate School of Electronic Science and Technology, Shizuoka University, Hamamatsu, Shizuoka 432-8011, Japan, [5]Department of Physiology, Hamamatsu University School of Medicine, Hamamatsu, Shizuoka 431-3192, Japan, [6]Laboratory for Memory and Learning, Brain Science Institute, RIKEN (Institute of Physical and Chemical Research), Wako-shi, Saitama 351-0198, Japan, [7]Department of Pharmacology, Graduate School of Medicine, Kyoto University, Sakyo, Kyoto 606-8501, Japan, and [8]Banyu Tsukuba Research Institute (Merck), Tsukuba, Ibaragi 300-2611, Japan

Na^+, K^+-ATPase α2 subunit gene (*Atp1a2*) knock-out homozygous mice (*Atp1a2*$^{-/-}$) died immediately after birth resulting from lack of breathing. The respiratory-related neuron activity in *Atp1a2*$^{-/-}$ was investigated using a brainstem–spinal cord *en bloc* preparation. The respiratory motoneuron activity recorded from the fourth cervical ventral root (C4) was defective in *Atp1a2*$^{-/-}$ fetuses of embryonic day 18.5. The C4 response to electrical stimulation of the ventrolateral medulla (VLM) recovered more slowly in *Atp1a2*$^{-/-}$ than in wild type during superfusion with Krebs' solution, consistent with the high extracellular GABA in brain of *Atp1a2*$^{-/-}$. Lack of inhibitory neural activities in VLM of *Atp1a2*$^{-/-}$ was observed by optical recordings. High intracellular Cl^- concentrations in neurons of the VLM of *Atp1a2*$^{-/-}$ were detected in gramicidin-perforated patch-clamp recordings. The α2 subunit and a neuron-specific K-Cl cotransporter KCC2 were coimmunoprecipitated in a purified synaptic membrane fraction of wild-type fetuses. Based on these results, we propose a model for functional coupling between the Na^+, K^+-ATPase α2 subunit and KCC2, which excludes Cl^- from the cytosol in respiratory center neurons.

Key words: **Na, K-ATPase; KCC2; respiratory neuron; brainstem–spinal cord preparation; $[Cl^-]_i$; GABA**

Introduction

The Na^+, K^+-ATPase (sodium pump) is a plasma membrane protein essential for maintaining Na^+ and K^+ gradients across the animal cell membrane. Glucose and amino acids, calcium ion, and various neurotransmitters are transported using the Na^+ gradients generated by this pump. The ion gradients are also critical to maintain osmotic balance and cytosolic pH and to support and modulate electrical activity of excitable cell membrane. The pump consists of α and β subunits. Four α isoforms (α1, α2, α3, and α4) have been identified in mammals (for review, see Lingrel et al., 2003). Each isoform exhibits unique tissue distribution and expression pattern during development, suggesting its tissue- and developmental stage-specific function. The α1 isoform gene is the housekeeping gene that is expressed ubiquitously and is indispensable for early embryonic development. The α2 isoform gene is expressed specifically and abundantly in skeletal muscle, heart, and brain. The mRNA of the α2 isoform is distributed throughout most regions of the brain at embryonic day 9.5 (E9.5) (Herrera et al., 1994). At the time of birth, the α2 isoform exists in neuronal cell bodies at all levels in the brain, as well as in glial cells (Moseley et al., 2003). With the maturation of the nervous system, the distribution of α2 isoform becomes gradually limited to glial cells, arachnoid membrane, and a few types of neurons in the adult (Sweadner, 1992; Peng et al., 1997). The α isoforms are differentially distributed in the plasma membrane compartments at a single-cell level of various tissues; the α1 isoform is distributed throughout the plasma membrane, whereas the α2 and α3 localize in more specific areas, such as plasma membrane regions overlying junctional sarcoplasmic and endoplasmic reticulums (Lingrel et al., 2003; Lencesova et al., 2004; Shelly et al., 2004). Moreover, each isoform shows different affinity for ouabain, kinetic properties for ion transport, and sensitivity to Ca^{2+} (Sweadner, 1989; Jewell and Lingrel, 1991; Blanco et al., 1995; Golovina et al., 2003).

The α2 subunit-deficient (*Atp1a2*$^{-/-}$) fetuses displayed selective neuronal apoptosis in the amygdala/piriform cortex (Ikeda et al., 2003) and died immediately after birth as a result of severe motor deficits that also abolished respiration. The aim of the present study was to determine the molecular mechanism of apnea in *Atp1a2*$^{-/-}$. The lack of α2 subunit causes functional impairment of the medullary respiratory center neurons. We observed high intracellular Cl^- concentrations ($[Cl^-]_i$) in neurons

Received July 19, 2004; revised Sept. 19, 2004; accepted Oct. 19, 2004.

This work was supported by the Narishige Neuroscience Research Foundation (K.I.) and by a grant from the Ministry of Education, Culture, Sports, Science and Technology of Japan. We thank S. Kamata, Y. Gotoh, K. Mogi, and K. Takase for their technical assistance.

Correspondence should be addressed to Dr. Kiyoshi Kawakami, Division of Biology, Center for Molecular Medicine, Jichi Medical School, Kawachi, Tochigi 329-0498, Japan. E-mail: kkawakam@jichi.ac.jp.

DOI:10.1523/JNEUROSCI.2909-04.2004

 0270-6474/04/2410693-09$15.00/0

of the respiratory center in E18.5 *Atp1a2*$^{-/-}$. The α2 subunit and a neuron-specific K-Cl cotransporter KCC2 were coimmunoprecipitated using a purified synaptic membrane fraction of E18.5 wild-type brain. Based on these results, we propose a model for functional coupling between the α2 subunit and KCC2, which excludes Cl^- from the cytosol in neurons. The results provide evidence that the Na^+, K^+-ATPase α2 subunit is critical for the function of respiratory center neurons at birth. Furthermore, the α2 isoform plays a key role for exclusion of Cl^- and maintenance of Cl^- homeostasis in neurons, and this role does not seem to be compensated by α1 and α3 isoforms.

Materials and Methods

Construction of Atp1a2 *targeting vector and generation of mutant mice.* Mouse genomic DNA containing exons 2 and 3 of the *Atp1a2* was isolated by screening a 129/Sv mouse genomic FIXII library (Stratagene, La Jolla, CA) using a rat *Atp1a2* cDNA probe [nucleotide positions 71–770 according to Shull et al. (1986)]. A ~8.5 kb *Hin*fI-*Sal*I fragment containing exons 2 and 3 was isolated and subcloned in pBlueScript KS (Stratagene). A PGKneobpA cassette (see Fig. 1*A*, neo) was inserted into a *Xho*I site in an opposite orientation, which was introduced in exon 2. The bacterial diphtheria toxin subunit gene (see Fig. 1*A*, DTA) driven by the phosphoglycerate kinase I gene promoter was inserted downstream of *Sal*I site. Embryonic stem (ES) cells (RW4 ES cell line) were electroporated with the linearized targeting vector. G418-resistant ES clones were screened by PCR using primers 5′-GGGAGAGACAGACACGGAGGAAGATGAC-3′ and 5′-TCGTGCTTTACGGTATCGCCGCTCCCGATT-3′. Homologous recombinant candidates were verified by Southern hybridization using the probe shown in Figure 1*A*. Chimeras were generated by injecting the recombinant ES cells into C57BL/6J blastocysts and transferred to multicross hybrid (CLEA Japan, Tokyo, Japan) foster mothers. *Atp1a2*$^{+/-}$ was backcrossed 10–12 generations to the C57BL/6. In every experiment, mice from each genotype were littermates and of isogenic genetic background. RNA was isolated from brains of E18.5 fetuses by homogenizing in ISOGEN (Nippon Gene, Tokyo, Japan). Reverse transcription (RT)-PCR was performed using OneStep RT-PCR Kit (Qiagen, Düsseldorf, Germany) with 100 ng of RNA and primers for the α2 subunit (5′-AGGCGGTGTGGTCTTGGGAT and 5′-CCACCCCCATTTTCCGCAGT) and for β-actin (5′-TGGTGGGAATGGGTCAGA and 5′-CCATCTCTTGCTCGAAGTC). Microsome fractions were prepared from each genotype as described previously (Ikeda et al., 2003). Then, 30 μg protein samples were immunoblotted as described previously (Ikeda et al., 2003). Antibodies for α1 subunit (Upstate Biotechnology, Lake Placid, NY), α2 subunit (Ikeda et al., 2003), and α3 subunit (Upstate Biotechnology) were used.

Recording of neural activity from the fourth cervical nerve root. Experiments were performed using brainstem–spinal cord preparations from E18.5 fetuses. Under deep ether anesthesia, the brainstem–spinal cords were isolated under dissection microscopy and placed in a recording chamber as described previously (Onimaru and Homma, 2003). The preparation was superfused at a rate of 3.0 ml/min with a modified Krebs' solution containing the following (in mM): 124 NaCl, 5.0 KCl, 1.2 KH_2PO_4, 2.4 $CaCl_2$, 1.3 $MgCl_2$, 26 $NaHCO_3$, and 30 glucose, pH 7.4 (equilibrated with 95% O_2 and 5% CO_2, at 26–27°C). Respiratory activity was recorded extracellularly from either the ventral C4 or C5 root using a glass suction electrode. Adrenaline (Sigma, St. Louis, MO) was added to the superfusate. For electrical stimulation (100 μsec, 10–30 μA), a tungsten electrode (tip diameter, 50 μm) with a resistance of 2 MΩ was inserted into the ventrolateral medulla (VLM). Respiratory activity monitored at the fourth cervical ventral root (C4) nerve root was high-pass filtered with a 0.3 sec time constant. The response was monitored under superfusion with modified Krebs' solution for >1 hr, when the level of response reached a plateau.

Optical recordings. The brainstem–spinal cord preparation was placed in a modified Krebs' solution containing a fluorescent voltage-sensitive dye (50 μg/ml Di-2-ANEPEQ; Molecular Probes, Eugene, OR) for 40–50 min. After being stained, the preparation was placed with the ventral surface up in a 1 ml perfusion chamber, which was mounted on a fluorescence microscope (BX50WIF-2; Olympus Optical, Tokyo, Japan). The preparation was superfused continuously at 2–3 ml/min with a modified Krebs' solution containing 5 μM adrenaline. Neuronal activity in the preparation was detected as a change in fluorescence of the voltage-sensitive dye by means of an optical recording apparatus (MiCAM01; Brain Vision, Tsukuba, Japan) as described previously (Onimaru and Homma, 2003). Most recordings were performed with an acquisition time of 20 msec. Fluorescence signals for 6.8 sec per trial, including 1.7 sec before the initiation of the inspiratory burst, were totaled and averaged 40–50 times; C4 inspiratory activity was used as the trigger. The fluorescence changes were expressed as a ratio (percentage, fractional changes) of the fluorescence intensity to that of the reference image. The differential image, processed with a software-spatial filter for 2 × 2 pixels, was represented by a pseudocolor display in which red corresponded to a decrease in fluorescence, meaning membrane depolarization. For representation of the time course of the fluorescence change in the region of interest, optical signals were inverted.

Measurements of GABA content. Preparation of whole brain and measurement of GABA content were described previously (Ikeda et al., 2003). For the measurement of extracellular GABA content in the brain, the whole brain was immediately removed from the decapitated fetus, cut into four blocks, and placed on a well of a 24-well tissue culture dish with 300 μl of oxygenated modified Krebs' solution. The perfusate was collected and replaced with 300 μl of fresh solution every 5 min. The perfusates collected in the first 20 min were combined, and GABA content was measured by reversed-phase HPLC and fluorimetric detection after derivatization with *o*-phthaldialdehyde as described previously (Ikeda et al., 2003).

Gramicidin-perforated patch-clamp recordings from brain-slice preparation. The procedures used for preparing mouse brain slices containing the facial nucleus were similar to those described previously (Toyoda et al., 2003). After the pregnant mice had been deeply anesthetized by inhalation of halothane, they were cesarean sectioned. The fetuses (E18.5) were decapitated, and the brain blocks were quickly removed and placed in cold (4°C), oxygenated artificial CSF (ACSF) containing (in mM): 126 NaCl, 2.5 KCl, 1.25 NaH_2PO_4, 2 $MgSO_4$, 2 $CaCl_2$, 26 $NaHCO_3$, and 20 glucose. Coronal slices (400 μm) were cut in ACSF using a vibratome. The slices were transferred to a recording chamber attached to the stage of a microscope (BH2; Olympus Optical) and continuously perfused with the oxygenated ACSF at a flow rate of 2 ml/min and temperature of 30°C. Slices were allowed to recover for 30 min before recordings. During voltage-clamp recording, 0.5 μM tetrodotoxin (Sigma) was added to block Na^+-dependent action potentials, and CGP55845 [(2*S*)-3-[[(1*S*)-1-(3,4-dichlorophenyl)ethyl]amino-2-hydroxypropyl](phenylmethyl)phosphinic acid] (Tocris Cookson, Ellisville, MO) was added to antagonize $GABA_B$ receptors. Gramicidin-perforated patch-clamp recordings (Abe et al., 1994) were performed as described previously (Toyoda et al., 2003; Yamada et al., 2004). Neurons in facial nucleus in the slices were viewed on a monitor via a 40× water immersion objective lens with infrared differential interference contrast filter and a CCD-camera (C2400–79H; Hamamatsu Photonics, Shizuoka, Japan). Real-time video images were contrast enhanced by a video processor (Argus-20; Hamamatsu Photonics). Patch electrodes were fabricated from borosilicate capillary tubing with diameter of 1.5 mm (Garner Glass, Claremont, CA) using a Narishige (Tokyo, Japan) PP-83 vertical puller. The electrode resistance ranged from 3 to 4.5 MΩ. The pipette solution contained the following (in mM): 150 KCl and 10 HEPES-KOH, pH 7.3. Gramicidin (Sigma) was dissolved in dimethylsulfoxide (10 mg/ml) and then diluted in the pipette filling solution to a final concentration of 5–10 μg/ml just before the experiment. Membrane currents and membrane potentials were recorded with the Axopatch 1D amplifier and digitized at 5–10 kHz by the use of Digidata 1332A data acquisition system (Axon Instruments, Union City, CA). Data were acquired with pClamp8 software (Axon Instruments) and stored on the hard disk for off-line analysis with Clampfit8 (Axon Instruments). To measure the reversal potential for the GABA-induced current ($E_{GABA\text{-}A}$), voltage steps were applied, and 50 μM GABA (Sigma) was pressure applied for 10–50 msec through a patch pipette to the soma of the recorded neurons at each membrane potential. Peak current responses for each voltage were plotted, and the data were fit using KyPlot software (Kyence, Osaka, Japan).

Estimation of intracellular chloride concentration. The series resistance (estimated from the peak transient during a 10 mV test pulse given before each trial) and the amplitude of the current (before baseline correction) 100–200 msec from the time of the pressure application were used to calculate the voltage error caused by uncorrected series resistance. The baseline current (determined at 20 msec before the time of the pressure pulse) was subtracted from the absolute current amplitude (baseline − corrected traces). To obtain *I–V* curves from gramicidin recordings, the membrane potential values were corrected for voltage drop across series resistance: $V_{corr} = V_{com} - I_{clamp} \times R_s$ where V_{com} is command potential, I_{clamp} is clamp current, and R_s is series resistance (<40 MΩ). These values were plotted as a function of the series resistance-corrected membrane potential. The $[Cl^-]_i$ was thus calculated from the $E_{GABA\text{-}A}$ according to the Nernst equation.

Estimation of driving force for K^+ in intact cells prepared from E18.5 brains. The method used to estimate the driving force for K^+ entailed measurement of the reversal potential of K^+ currents in cell-attached mode and was identical to that described previously (Verheugen et al., 1999). At a given K^+ concentration in the pipette solution (in mM: 120 KCl, 11 EGTA, 1 $CaCl_2$, 2 $MgCl_2$, and 10 HEPES, adjusted to pH 7.26 with 35 KOH), the K^+ currents reverse when the pipette potential (V_{pip}) cancels the difference between V_m and the equilibrium potential for K^+ (E_K) across the patch. Therefore, the cell holding potential ($-V_{pip}$) at which the K^+ current reverses direction provides a direct measure of the driving force for K^+ in an intact cell ($-V_{pip} = E_k - V_m$). Depolarizing voltage ramps of 20 msec duration were applied, at an interval of 2–2.5 sec, from −100 to +200 mV. For analysis of currents evoked by the ramp stimulation, a correction was made for a leak component by linear fit and extrapolation of the closed level.

Preparation of purified synaptic membrane fraction and coimmunoprecipitation experiment. Whole brains of E18.5 mice were homogenized in 9 ml/gm tissue of sucrose buffer (0.32 M sucrose and 10 mM Tris-HCl, pH 7.2) with a Potter-Teflon homogenizer (800 rpm, 12 times) with cooling at 0°C. The homogenates were spun at 1000 × *g* for 10 min at 4°C. The supernatant (S_1) was collected and centrifuged at 15,000 × *g* for 30 min at 4°C. The pellet (P_2) was resuspended with sucrose buffer and homogenized four times with Dounce homogenizer at 0°C, followed by centrifugation at 15,000 × *g* for 30 min at 4°C. The pellet (P_2') was resuspended in sucrose buffer in 3 ml/gm tissue and placed at the top of three layers of Ficoll (17, 13, and 7.5% in 0.32 M sucrose buffer). The sample was subjected to centrifugation at 63,000 × *g* for 45 min at 4°C. The fraction in the 13–7.5% interface (light synaptosome fraction) was collected. To remove the Ficoll, the fraction was diluted four times in sucrose buffer and centrifuged at 15,000 × *g* for 30 min at 4°C. The pellet (purified synaptosome) was suspended with 10 ml/gm tissue in hypo-osmotic buffer (5 mM Tris-HCl and 0.1 mM EDTA, pH 8.0) and passed through a 22 gauge needle five times, followed by incubation in 4°C for 1 hr. The sample was then centrifuged at 100,000 × *g* for 30 min at 4°C. The pellet (crude synaptic membrane) was resuspended in 0.32 M sucrose buffer, placed on the top of four layers of sucrose (1.3, 1.0, 0.8, and 0.6 M), and subjected to centrifugation at 63,000 × *g* for 1.5 hr at 4°C. The fraction in the 0.6–0.8 M interface was purified synaptic membrane, which was highly enriched in Na^+, K^+-ATPase α2 subunit (K. Ikeda, unpublished observations). This purified synaptic membrane fraction was used for coimmunoprecipitation assay. Next, 25 μg of protein of purified synaptic membrane fraction was precleared by incubation with equilibrated 150 μl Protein A Sepharose FF beads (Amersham Biosciences, Uppsala, Sweden) in a binding buffer [0.2 gm/l KCl, 0.2 gm/l KH_2PO_4, 8 gm/l NaCl, 2.16 gm/l $NaH_2PO_47H_2O$, and protease inhibitor mixture tablets (Roche Diagnostics, Mannheim, Germany)] at 4°C. The recovered samples were incubated with appropriate antibodies (5 μg) in the binding buffer with 0.2% Tween 20 and rotation for 10 hr at 4°C. The samples were further incubated with fresh equilibrated 150 μl Protein A Sepharose FF beads for 4 hr at 4°C. After incubation, the beads were washed four times with a washing buffer (145 mM NaCl, 10 mM NaH_2PO_4, 10 mM sodium azide, and 0.5% Tween 20, pH 7.0). Immunoprecipitated proteins were then extracted with 150 μl of 2× Laemmli sample buffer and boiled for 5 min. Next, 25 μl of 150 μl was subjected to separation on SDS polyacrylamide gels. Immunoblotting was performed as described previously (Ikeda et al., 2003). Antibodies used for immunoprecipitation and immunoblotting in Figure 4 were affinity-purified polypeptide antibodies against mouse Na^+, K^+-ATPase α2 subunit (Ikeda et al., 2003), KCC2 (CDNEEKPEEEVQLIH, which covers amino acids 961–975 of the mouse KCC2 protein), and Six1 (RSSNYSLPGLTASQPSHGLQ, which covers amino acids 242–261 of the mouse nuclear transcription factor, Six1, as a control). Affinity purification of antibodies was performed by absorption on covalently linked peptide columns.

In situ *hybridization and Northern blot analyses for KCC2 expression.* The *in situ* hybridization histochemistry was performed as described previously (Toyoda et al., 2003), with the following modifications. The 16-μm-thick frozen sections were prepared from each genotype fetuses. Antisense oligo cDNA probe and a sense oligo cDNA probe (complementary to antisense) for KCC2 mRNA were designed as follows; KCC2 antisense, 5′-CCCGAAGAGACAGCGTGTGACAATGAGGAGAAGCCA-3′; KCC2 sense, 5′-TGGCTTCTCCTCATTGTCACACGCTGTCTCTTCGGG-3′. The Northern blot analysis was performed with 30 μg of total RNA isolated from brains of each genotype. The fragment containing KCC2 coding sequence (CDS) was obtained by RT-PCR using primers (5′-GGAAGCTTATGCTCAACAACCTGACGGAC and 5′-GGGGAT-CCTCAGGAGTAGATGGTGATGAC) and poly(A)$^+$ RNA of mouse E11 (Sigma) as a template and subcloned to pBluescript (Stratagene). The entire region was verified by sequencing. The fragment spanning from 2773 to 3143 of CDS (DNA Data Bank of Japan accession number BC054808) was used as a probe.

Statistical analysis and ethical considerations. Data are presented as mean ± SEM. Data shown in Figures 2*B* and 3*D* and the estimated K^+ driving force in Results were compared using the Student's *t* test. In the experiment shown in Figure 2*C*, differences between groups were examined for statistical significance using one-way ANOVA, followed by Scheffe's PLSD test. A p value <0.05 denoted the presence of a statistically significant difference. All experimental protocols described in the present study were approved by the Ethics Review Committee for Animal Experimentation of Jichi Medical School.

Results

Atp1a2$^{-/-}$ mice die immediately after birth resulting from lack of respiratory neural activity

To examine the roles of Na^+, K^+-ATPase α2 subunit in the nervous system during development, we produced two lines of mice with defective α2 subunit gene. A neomycin-resistant gene cassette (*neo*) was inserted in exon 2 in the first (named N-KO mice) (Fig. 1*A*), whereas a *neo* was inserted in exon 21 in the second (named C-KO mice) (Ikeda et al., 2003). In either line of homozygous knock-out mice, no α2 isoform was detected in the membrane fraction of the brain (Ikeda et al., 2003) (Fig. 1*D*). Both N-KO and C-KO homozygotes survived until birth with no apparent phenotypic abnormalities and showed undisturbed development, apart from severe motor deficits before and at birth (Ikeda et al., 2003) (data not shown). They died immediately after birth resulting from lack of respiratory activity. The C-KO knock-out homozygotes show severe neuronal apoptosis in selected brain regions: the amygdala and piriform cortex, at E18.5–E19 (Ikeda et al., 2003). In contrast, these regions are intact in the N-KO knock-out homozygotes (data not shown). These observations suggest that the degeneration in the amygdala and piriform cortex is not the cause of akinesia and apnea that were observed in both lines of homozygotes.

In this study, we addressed the molecular mechanism of apnea at birth observed in *Atp1a2*$^{-/-}$ neonates by analyzing the N-KO knock-out mice. Exon 2 contains the translation start codon of ATG. The targeted allele was verified by PCR (data not shown) and Southern hybridization (Fig. 1*B*). Disruption of α2 subunit expression in the brain was confirmed by RT-PCR and Northern blot analyses (Fig. 1*C* and data not shown). We also confirmed the lack of α2 subunits in the microsome fraction prepared from

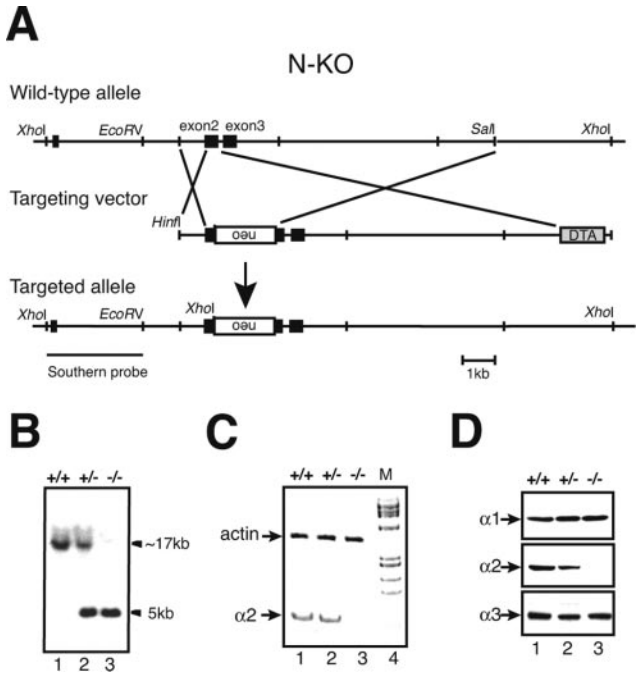

Figure 1. Targeted disruption of the mouse *Atp1a2*. *A*, Targeting strategy for mutating the Na^+, K^+-ATPase $\alpha 2$ subunit gene (*Atp1a2*). Exons are represented as black boxes. A neomycin-resistant gene cassette (neo, depicted as a white box) was inserted in the opposite orientation into exon 2, and a bacterial diphtheria toxin subunit gene (DTA, depicted as a gray box) was inserted for negative selection. The targeted allele was verified by PCR (data not shown) and Southern blot analyses with the indicated probe in *A*. *B*, Southern blot analysis of genomic DNA. The *Xho*I DNA fragments from the wild-type (~17 kb) and targeted (5 kb) alleles are shown. *C*, RT-PCR analysis of total RNA isolated from the E18.5 brain of each genotype. Positions of PCR products for the $\alpha 2$ subunit and β-actin as a control are indicated. Note that the $\alpha 2$ subunit PCR product is absent in *Atp1a2*$^{-/-}$ mice ($-/-$). *D*, A microsome fraction was prepared from the brains of E18.5 mice, and 40 μg of protein was analyzed by Western blotting with an anti-$\alpha 1$ (1:2000), an anti-$\alpha 2$ (1:1000), or an anti-$\alpha 3$ (1:2000) antibody. Note that the $\alpha 2$ subunit polypeptide is absent in *Atp1a2*$^{-/-}$ mice.

E18.5 brain by Western blotting (Fig. 1*D*). Heterozygous mice (*Atp1a2*$^{+/-}$) seemed normal, including life expectancy. On the other hand, homozygous mutant mice (*Atp1a2*$^{-/-}$) developed *in utero* and did not show any abnormalities in appearance. At birth, *Atp1a2*$^{-/-}$ were characterized by lack of spontaneous body movement and response to pinch. All *Atp1a2*$^{-/-}$ failed to breathe or showed gasping-like mouth opening two to three times at most (data not shown) and died within 10–15 min. Therefore, the fetuses were harvested at E18.5 by cesarean section.

The $\alpha 2$ subunit is abundantly expressed in neurons in the brainstem, including respiratory center (Moseley et al., 2003). The neural network for respiratory rhythm is genetically programmed and developed *in utero*, and newborn mammals breathe immediately after birth. This neural circuit is located rostrocaudally in the VLM of the lower brainstem. It produces rhythmic activity, which is transmitted to spinal motoneurons to generate a periodic contraction of respiratory muscles, such as diaphragm. As a measure of respiratory output, we recorded the respiratory activity from the C4, one of phrenic nerve motoneurons, in an *en bloc* brainstem–spinal cord preparation isolated from E18.5 mice (Ballanyi et al., 1999). Spontaneous rhythmic discharges related to inspiration were recorded in the wild types ($n = 23$) (Fig. 2*A*, top, *Atp1a2*$^{+/+}$) and heterozygotes (data not shown; $n = 18$) but were completely absent in the homozygotes ($n = 35$) (Fig. 2*A*, bottom, *Atp1a2*$^{-/-}$). The results were consistent with the observation that the homozygotes completely lacked the respiratory activity after birth.

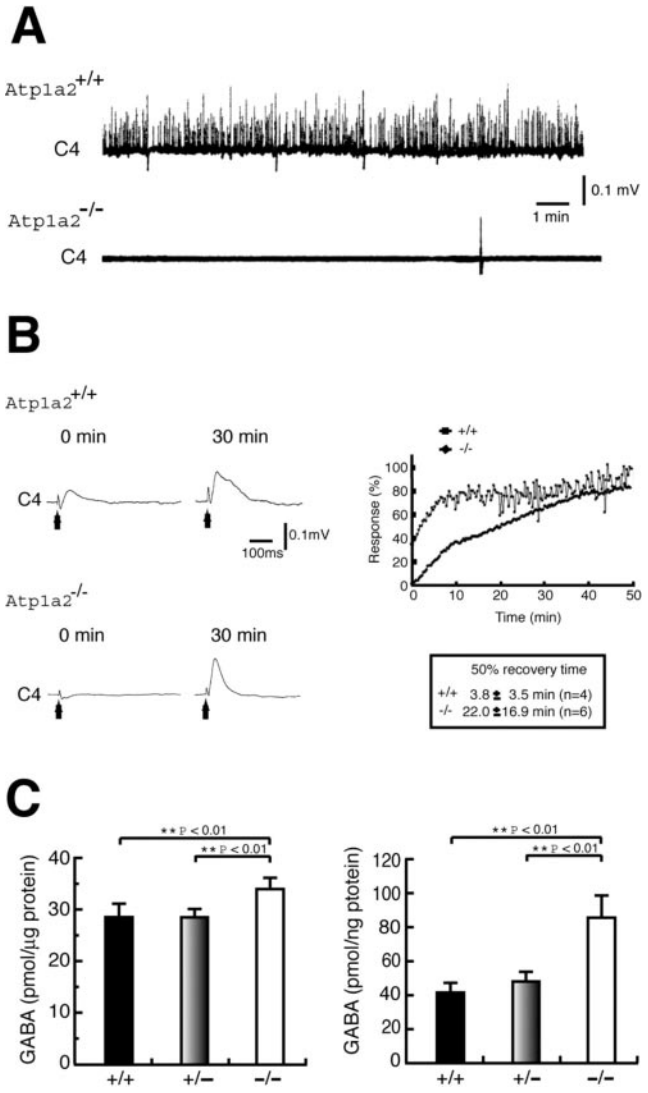

Figure 2. Recordings from brainstem–spinal cord preparation and GABA content in the brain. *A*, Examples of inspiration-related activity recorded from the cervical (C4) ventral root of isolated brainstem–spinal cord preparations from E18.5 fetuses. Preparations from wild-type fetuses (top, *Atp1a2*$^{+/+}$) showed spontaneous respiratory rhythm activity, which was absent in *Atp1a2*$^{-/-}$ preparation (bottom). Traces show raw filtered and integrated activities. *B*, Response to electrical stimulation of the VLM monitored by C4 nerve root recording in a brainstem–spinal cord preparation. Arrows indicate the time of stimulation. In *Atp1a2*$^{+/+}$, response was observed at 0 min, when the brainstem–spinal cord preparation was transferred to *in vitro*, whereas no response was observed at the same time point in *Atp1a2*$^{-/-}$. Responses were observed for both at 30 min. Representative time course of C4 response to VLM stimulation (right). The plateau level of response was set at 100% for each preparation. Note the lack of fluctuation of the response in *Atp1a2*$^{-/-}$, indicating the absence of spontaneous respiratory rhythm activity. The 50% of recovery time was significantly slower in *Atp1a2*$^{-/-}$ ($n = 6$) compared with that in *Atp1a2*$^{+/+}$ ($n = 4$), as shown in the box ($p < 0.05$). *C*, Left, GABA content was significantly higher in *Atp1a2*$^{-/-}$ whole brain than in *Atp1a2*$^{+/+}$ and *Atp1a2*$^{+/-}$ brains. The values of the whole brain were normalized for protein content. The mean values of GABA for *Atp1a2*$^{+/+}$ ($+/+$; $n = 5$), *Atp1a2*$^{+/-}$ ($+/-$; $n = 8$), and *Atp1a2*$^{-/-}$ ($-/-$; $n = 9$) are shown. Right, GABA content in the perfused fractions of the brain was significantly higher in *Atp1a2*$^{-/-}$ whole brain than in *Atp1a2*$^{+/+}$ and *Atp1a2*$^{+/-}$ brains. The mean total values of GABA in the perfused fractions during the first 20 min for the *Atp1a2*$^{+/+}$ ($+/+$; $n = 6$), *Atp1a2*$^{+/-}$ ($+/-$; $n = 8$), and *Atp1a2*$^{-/-}$ ($-/-$; $n = 9$) were normalized for input tissue protein amount. Data are mean ± SEM. $^{**}p < 0.01$.

We next examined the C4 reflex responses evoked by electrical stimulation of VLM. Respiratory neurons located in VLM are important for respiratory rhythm generation and inspiratory pattern generation (Ballanyi et al., 1999; Richter and Spyer, 2001). In

this experiment, the brainstem–spinal cord of E18.5 mice was isolated within 5 min of the cesarean section. During the recording, the brainstem–spinal cord preparation was superfused with oxygenated modified Krebs' solution at 26°C. In the wild type, the C4 response was observed at the very beginning of recording (0 min, i.e., 10 min after being killed) and was augmented at 30 min (Fig. 2*B*, top left, *Atp1a2*$^{+/+}$). The magnitude of response to electrical stimulation at 0 min was 30% of the plateau level and increased over time. The gradual augmentation of the response was interpreted as transition processes from "*in vivo* state" to "*in vitro* state" of the samples during superfusion, such as recovery from sample damage and release from repressed state. The response reached a plateau level within 10 min. Fluctuation of the plateau level was noticed after 20 min attributable to frequent spontaneous breathing-related neural activities (Fig. 2*B*, right, filled squares). In contrast, we could not detect any C4 responses to electrical stimulation at 0 min in homozygotes, although the response was detected at 30 min (Fig. 2*B*, bottom left, *Atp1a2*$^{-/-}$). The responses developed gradually over a period of 1 hr and reached a plateau level (Fig. 2*B*, right, filled rhombuses). The time for the half-maximum level of the reflex response was 3.8 ± 3.5 (mean ± SEM) min in the wild-type mice ($n = 4$) and 22.0 ± 16.9 min in the homozygous mice ($n = 6$). These results indicate that the neuronal circuitry from the VLM to C4 was preserved in the homozygotes, but the transition process was significantly slower in the homozygotes than in the wild types ($p < 0.05$). A likely explanation for the absence of the C4 response to electrical stimulation at the beginning of the recording and the slower transition process of the reflex response in the homozygotes is the presence of excess inhibitory substance(s) to neural activities *in vivo* (Ikeda et al., 2003). It is possible that superfusion of the preparation with modified Krebs' solution resulted in a washout of the putative inhibitory substances from the extracellular spaces and restoration of neural responses after 1 hr.

Consistent with the above notion, the whole-brain level of the inhibitory neurotransmitter GABA was significantly higher in the homozygous mice brain than in the heterozygous or wild-type mice at E18.5 (Fig. 2*C*, left). Furthermore, the levels of GABA in the perfusate were significantly higher in the homozygotes than that in the heterozygotes or wild types in the first 20 min perfusion (Fig. 2*C*, right). After 40 min perfusion, the levels of GABA in the superfusate were almost similar in the homozygotes, heterozygotes, and wild types (data not shown). We reported previously that the neurotransmitter reuptake process was impaired in the C-KO homozygous mice brain (Ikeda et al., 2003). The transporters eliminate the neurotransmitters from the extracellular space after excitation-induced vesicular release by the use of Na^+ gradient formed by the Na^+, K^+-ATPase α2 subunit (Ikeda et al., 2003). These results suggest that increased inhibitory substance GABA levels in the extracellular spaces are the reason for suppression of the respiratory rhythm generation in the homozygous mutants *in vivo*. This conclusion was supported by the observation that the lying-still homozygotes (just after birth, within 10 min) showed two to three gasping-like activities after intraventricular injection of bicuculline, a $GABA_A$ receptor antagonist ($n = 4$) (Ikeda, unpublished observations).

Defective inhibitory neural activity in respiratory neural network in *Atp1a2*$^{-/-}$ mice

Homozygous mice did not show any spontaneous rhythmic C4 activity, even after the reflex responses by stimulation of the VLM were recovered by superfusion (Fig. 2*B*, right). However, superfusion with modified Krebs' solution for 1 hr followed by bath application of stimulatory neuromodulators, such as adrenaline or substance P, induced regular inspiratory bursts in the homozygote (Fig. 3*A* and data not shown). The results imply that the neural network for inspiratory burst generation in the VLM was not severely defective in the homozygotes, consistent with the previous study (Moseley et al., 2003). However, the burst rate in the presence of 5 μM adrenaline was significantly lower in the homozygotes (2.4 ± 0.6 min^{-1}; $n = 10$) (Fig. 3*A*, bottom, *Atp1a2*$^{-/-}$) than that of the wild types (3.7 ± 0.8 min^{-1}; $n = 7$; $p < 0.05$) (Fig. 3*A*, top, *Atp1a2*$^{+/+}$). Failure of spontaneous respiratory rhythm generation in the homozygotes could be attributable to dysfunction of rhythm generator neurons that periodically trigger the inspiratory burst generation in the brainstem–spinal cord preparation.

To obtain additional insights into the underlying defects in the homozygous rhythm generator, we performed optical recordings to visualize respiratory neural activity from the ventral surface using voltage-sensitive dye (Onimaru and Homma, 2003) and compared the optical signals during adrenaline application between the homozygotes and the wild types (Fig. 3*B*). In these experiments, the brainstem–spinal cord preparation was perfused for >30 min before commencement of optical recording. Strong fluorescence changes at two regions of medulla were detected close to the peak of C4 inspiratory activity (indicated C4, purple traces). The fluorescence decreased (i.e., depolarization) in the wild-type ($n = 3$), heterozygous ($n = 6$; data not shown), and homozygous ($n = 5$) mice in the VLM spanning from the level just rostral to the IX/X cranial nerves to the caudal level of the rostral roots of the XII cranial nerves (Fig. 3*B*, top and bottom, red traces). The depolarization was detected 50 msec before the onset of C4 activity. This region approximately corresponds to the pre-Bötzinger complex (preBötC): the kernel of the circuit generating respiration neural activity (for review, see Feldman et al., 2003). The preBötC is necessary for generation of respiratory-related motor rhythm *in vivo* (Gray et al., 2001) and in the brainstem–spinal cord preparation (Smith et al., 1991). We observed an increase in the fluorescence (i.e., hyperpolarization) 100 msec after the peak of C4 activity in the wild type (Fig. 3*B*, top, blue trace) and heterozygote (data not shown) in the facial nucleus region. In contrast, the fluorescence decreased (i.e., depolarization) in the homozygous mice (Fig. 3*B*, bottom, blue trace). These results suggest impairment of the inhibitory neural activity in the ventral medulla and its transformation to excitatory activity in the *Atp1a2*$^{-/-}$ mice even after excess extracellular GABA was washed out.

GABA responses were depolarizing because of high $[Cl^-]_i$ in the homozygote

To determine the mechanism of impaired inhibitory neural activity in the homozygotes at a cellular level, we examined the response in the neurons of the facial nucleus region of E18.5 mice to GABA application (Fig. 3*C*). Gramicidin-perforated patch-clamp recordings in slice preparation were performed. Gramicidin was used as the membrane-perforating agent to allow the recording of whole-cell currents without impairment of $[Cl^-]_i$ (Abe et al., 1994). Pressure application of 50 μM GABA caused hyperpolarizing (inhibitory) potentials in the wild types and heterozygotes ($n = 3$) (Fig. 3*C*, top). In contrast, depolarization was observed in the homozygotes during GABA application ($n = 7$) (Fig. 3*C*, bottom). Remarkably, action potential firing was also observed in some of the homozygotes ($n = 2$).

$GABA_A$ receptor consists of ligand-gated Cl^- channel, in which the fast hyperpolarizing potential is mainly mediated by Cl^- and to a lesser extent by HCO^{3-} (Kaila, 1994; Barnard et al.,

1998; Brockhaus and Ballanyi, 1998). The depolarizing GABA response at fast phase has been attributed to various mechanisms. Recent studies have suggested that the Cl^- gradient is the dominant contributor to $GABA_A$-induced changes of depolarization–hyperpolarization during development (for review, see Ben-Ari, 2002; Owens and Kriegstein, 2002). Thus, the above observation could be reasoned by hypothesizing that $[Cl^-]_i$ is higher in the homozygote. We estimated resting membrane potentials of neurons in the facial motor nucleus region using the above setup. The mean resting membrane potential was -56.5 ± 7.3 mV for the wild types/heterozygotes ($n = 6$) and -62.8 ± 6.1 mV for the homozygotes ($n = 8$) (Fig. 3*D*, left); the difference between groups was not significant. Because of the existence of background spontaneous postsynaptic potential activities, the resting membrane potential of the wild types/heterozygotes showed a rather depolarizing tendency than that of the homozygotes. We next examined the reversal potential of $GABA_A$ receptor-mediated currents ($E_{GABA\text{-}A}$) of facial motor neurons. The membrane potential was set to different values by injection of direct currents during pressure application of 50 μM GABA. In neurons of the wild types/heterozygotes, $E_{GABA\text{-}A}$ was -64.6 ± 5.2 mV, whereas it was -48.7 ± 13.7 mV in neurons of the homozygotes. The mean values of $E_{GABA\text{-}A}$ were significantly less negative in the homozygotes ($p < 0.05$). The driving force, which was calculated by subtracting resting membrane potential from $E_{GABA\text{-}A}$ for each neuron, was -8.1 ± 7.0 mV for the wild types/heterozygotes and 14.0 ± 9.6 mV for the homozygotes ($p < 0.01$). The positive driving force of the homozygotes indicates the outward flow of Cl^- from the cytoplasm or the depolarization. The $[Cl^-]_i$ calculated from $E_{GABA\text{-}A}$ by the use of the Nernst equation (see Materials and Methods) was 11.5 ± 2.1 mM in the wild types/heterozygotes and 23.2 ± 12.6 mM in the homozygotes ($p < 0.05$). These results clearly demonstrate higher $[Cl^-]_i$ in neurons of the homozygotes than the wild types/heterozygotes.

Expression level of KCC2 is not altered in the homozygotes

A recent study identified a family of cation-chloride cotransporters (CCCs) that controls the chloride gradient across neurons (Payne et al., 2003). One of the CCCs, K^+-Cl^- cotransporter KCC2, is exclusively expressed in neurons and exhibits a high affinity for K^+ and extrudes

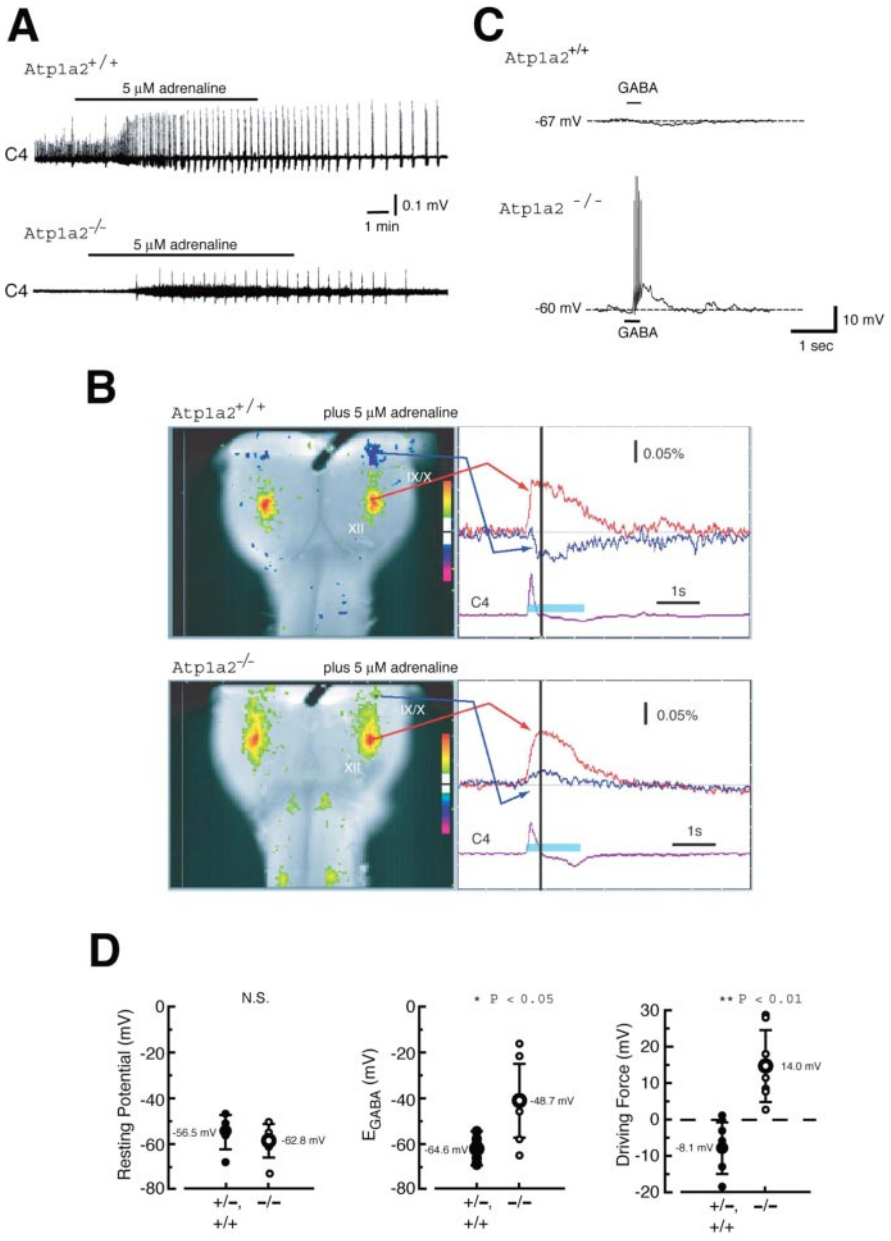

Figure 3. Electrical and optical recordings of respiratory neurons in the VLM. *A*, Representative trace showing the effect of bath application of 5 μM adrenaline (denoted by bars above the neuron tracing) on C4 activity in the brainstem–spinal cord preparation. The C4 activity emerged in the *Atp1a2*$^{-/-}$ in the presence of adrenaline (bottom). *B*, Left, Fluorescence changes in the optical recordings of respiratory neuron activity. Optical image of respiratory neuron activity near the C4 peak (at black vertical line in the right trace) superimposed on the ventral surface of the medulla. IX/X and XII are the IX/Xth and the XIIth cranial nerve roots, respectively. Right, Tracing of fluorescence changes at two different locations on the medulla: blue, at the level just rostral to the IX/Xth cranial roots; red, at the level of the rostral roots of the XIIth cranial nerve. Fluorescence decrease (i.e., depolarization) is upward, and fluorescence increase (i.e., hyperpolarization) is downward. The purple tracing represents C4 inspiratory activity. The light-blue bar on the C4 tracing denotes the inspiratory phase. The fluorescence change at the level just rostral to the IX/Xth cranial roots (blue tracings) represents hyperpolarization in the wild type (top, *Atp1a2*$^{+/+}$) and depolarization in the homozygote (bottom, *Atp1a2*$^{-/-}$). Results are the average of 40–50 respiratory cycles triggered by C4 inspiratory activity. 0.05%, Calibration for fluorescence change. *C*, Gramicidin-perforated patch-clamp recordings in the current-clamp mode at resting membrane potential. GABA (50 μM) hyperpolarized *Atp1a2*$^{+/+}$ facial nucleus neurons (top; $n = 3$) but depolarized those of *Atp1a2*$^{-/-}$ (bottom; $n = 7$). Representative tracings are shown. Note the action potential firing in response to GABA application in *Atp1a2*$^{-/-}$, indicating the excitatory action of GABA. GABA was applied using pressure pulses of 35–100 kPa for 10–50 msec. Reversal potentials for $GABA_A$-evoked currents were obtained from the same neurons in voltage-clamp mode. *D*, Resting membrane potential and reversal potential of $GABA_A$ receptor-mediated current ($E_{GABA\text{-}A}$) of facial motoneurons of E18.5 mice in slice preparation. Resting membrane potential was not significantly different between *Atp1a2*$^{+/+}$/*Atp1a2*$^{+/-}$ (filled circles; -56.5 ± 7.3 mV; $n = 6$) and *Atp1a2*$^{-/-}$ (open circles; -62.8 ± 6.1 mV; $n = 8$), whereas $E_{GABA\text{-}A}$ was significantly shifted in positive direction in *Atp1a2*$^{-/-}$ (-48.7 ± 13.7 mV) compared with that of *Atp1a2*$^{+/+}$/*Atp1a2*$^{+/-}$ (-64.6 ± 5.2 mV; $p < 0.05$). The driving force for $GABA_A$ receptor-mediated currents was positive in *Atp1a2*$^{-/-}$ (14.0 ± 9.6 mV) but negative in *Atp1a2*$^{+/+}$/*Atp1a2*$^{+/-}$ (-8.1 ± 7.0 mV), indicating that $GABA_A$ receptor-mediated actions were reversed to depolarization in homozygote.

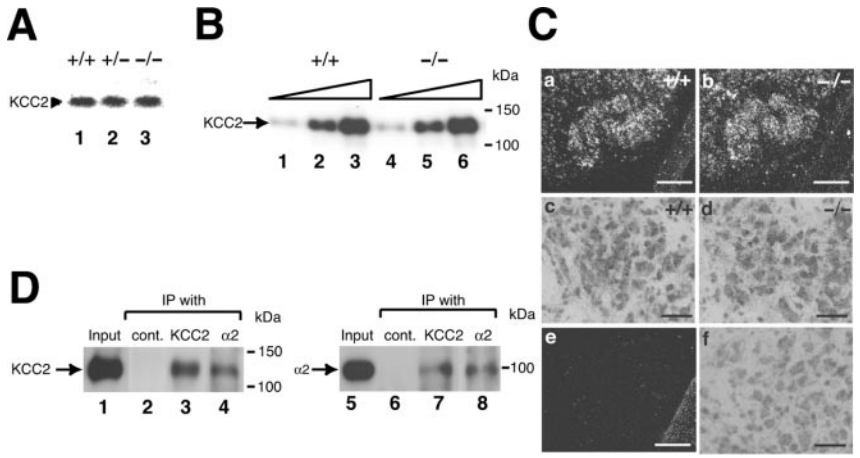

Figure 4. Analysis of KCC2 mRNA and protein in the brain. *A*, Northern blot analysis of KCC2 expression in E18.5 whole brains of *Atp1a2*$^{+/+}$, *Atp1a2*$^{+/-}$, and *Atp1a2*$^{-/-}$. In these studies, 30 μg of total RNA was hybridized. No difference was noted in the intensity of detected signals. Arrowhead indicates the KCC2 signal with the size of ~5.3 kb. *B*, Western blotting of KCC2 using purified synaptic membrane fraction from E18.5 whole brain of *Atp1a2*$^{+/+}$ (lanes 1–3) and *Atp1a2*$^{-/-}$ (lanes 4–6). The amount of protein added to each lane was 3 μg (lanes 1, 4), 10 μg (lanes 2, 5), and 30 μg (lanes 3, 6). Similar amounts of KCC2 protein were detected between *Atp1a2*$^{+/+}$ and *Atp1a2*$^{-/-}$ in the lanes in which the same amount of proteins was loaded. *C*, *In situ* hybridization of KCC2 mRNA in facial nucleus of E18.5 *Atp1a2*$^{+/+}$ and *Atp1a2*$^{-/-}$. *a*, *b*, Dark-field photomicrographs show that the expression of KCC2 mRNA in *Atp1a2*$^{-/-}$ (*b*) was comparable with that of *Atp1a2*$^{+/+}$ (*a*). *c*, *d*, Bright-field photomicrographs counterstained with thionin show the localization of KCC2 mRNA hybridization signals in facial motoneurons. The KCC2 mRNA distribution in *Atp1a2*$^{+/+}$ mice (*c*) was comparable with that of *Atp1a2*$^{-/-}$ mice (*d*). *e*, *f*, Sense probe show no hybridization signals in facial nucleus of an E18.5 *Atp1a2*$^{+/+}$ in dark-field (*e*) and light-field (*f*) photomicrographs. Scale bars: *a*, *b*, *e*, 200 μm; *c*, *d*, *f*, 50 μm. *D*, Coimmunoprecipitation of KCC2 and α2 subunit in synaptic membrane isolated from wild-type E18.5 mouse brain. Purified synaptic membrane fraction was immunoprecipitated with control anti-Six1 (lanes 2, 6), anti-KCC2 (lanes 3, 7), and anti-α2 (lanes 4, 8) antibodies. Protein (1.5 μg) was loaded on lanes 1 or 5 as an input. After blotting, KCC2 was probed with anti-KCC2 (lanes 1–4), and α2 subunit was probed with anti-α2 (lanes 5–8) antibodies. Note the presence of KCC2 in the precipitates of anti-α2 (lane 4) and α2 subunit in the precipitate of anti- KCC2 (lane 7) but not in the control antibody (lanes 2, 6).

Cl^- from cells under physiological conditions (Payne et al., 1996; Payne, 1997; Williams et al., 1999). Low KCC2 expression correlates with a decrease in the GABAergic driving force (Rivera et al., 1999; Nabekura et al., 2002; Toyoda et al., 2003) and developmental shift in GABA action, and thus $[Cl^-]_i$ correlates with the KCC2 expression level (Kaila, 1994; Rivera et al., 1999; Ben-Ari, 2002; Payne et al., 2003; Stein et al., 2004; Yamada et al., 2004). The KCC2 knock-out mice die immediately after birth because of the anomalous excitatory actions of GABA and glycine, which lead to motor function deficits, including respiration (Hübner et al., 2001). The above background prompted us to examine the KCC2 expression level in *Atp1a2*$^{-/-}$ mice. Contrary to our expectation, the expression level of KCC2 was not altered among *Atp1a2*$^{+/+}$, *Atp1a2*$^{+/-}$, and *Atp1a2*$^{-/-}$ when examined by Northern blot analysis with the total RNA prepared from whole brain of E18.5 mice (Fig. 4*A*). There was also no apparent difference in the expression of KCC2 in the facial nucleus region, which includes respiratory neurons, by *in situ* hybridization between the wild type and homozygote (Fig. 4*C*). We further checked the KCC2 protein content in the purified synaptic membrane fraction from E18.5 brain and found no decrease in the homozygotes (Fig. 4*B*). These results indicate that the lack of the sodium pump α2 subunit in neurons does not cause downregulation of KCC2, in contrast to neuronal injury such as axotomy (Nabekura et al., 2002; Toyoda et al., 2003).

The energy for the net transport of KCC2 is derived from the K^+ gradient generated by Na^+, K^+-ATPase (for review, see Payne et al., 2003). If the intracellular K^+ concentration ($[K^+]_i$) is low in the absence of α2 subunit, it would result in KCC2 dysfunction. To address this possibility, we performed cell-attached recordings to determine the driving force for K^+ in intact cells by measuring the reversal potential of K^+ currents (Verheugen et al., 1999), because the exact composition of intracellular ions cannot be mimicked by that of the pipette solution. To activate the voltage-dependent K^+ channels, voltage ramps from −100 to +200 mV were repeated at 0.5 Hz without any significant inactivation of K^+ channels. At the reversal of K^+ current, the holding potential provides an estimate of the driving force for K^+ in intact cells. The estimated K^+ driving forces given an extracellular K^+ concentration of 155 mM were −77.6 ± 9.4 mV for the wild types/heterozygotes (n = 13 cells from four fetuses) and −79.1 ± 10.8 mV for the homozygotes (n = 13 cells from three fetuses), which were not significantly different. The data agreed with those shown in Figure 3*D* (left), which showed no difference in the average resting membrane potential between the wild types/heterozygotes and homozygotes. We concluded that the lack of α2 subunit does not affect cytosomal $[K^+]_i$.

We therefore hypothesized that the α2 subunit of Na^+, K^+-ATPase provides local K^+ gradient used by KCC2 in neurons. If this were the case, KCC2 and α2 subunit would be localized in close proximity of the synaptic membrane. To test this possibility, coimmunoprecipitation assays were performed using purified synaptic membrane fractions prepared from E18.5 mouse brain. The use of an antibody against KCC2 did not only immunoprecipitate KCC2 but also the α2 subunit (Fig. 4*D*, lanes 3, 7). Reciprocal experiments showed immunoprecipitation of KCC2 and the α2 subunit with an antibody against α2 subunit (lanes 4, 8). In contrast, neither KCC2 nor α2 subunit was immunoprecipitated with control antibodies (lanes 2, 6). The results suggest that the KCC2 are located adjacent to the α2 subunit on the synaptic membrane in the neuron. We concluded that K^+ gradient, which fuels the extrusion of Cl^- by KCC2, is generated by Na^+, K^+-ATPase, which contains the α2 subunit in respiratory center neurons in the perinatal period.

Discussion

Defective respiratory rhythm generation in *Atp1a2*$^{-/-}$

The lack of spontaneous respiratory activity in the homozygotes is attributed to defects of the brainstem respiratory neurons, probably as a result of elevated $[Cl^-]_i$. Excess extracellular GABA may be caused by reduced clearance by the GABA transporter, which is functionally coupled to the α2 subunit (Fig. 2*C*) (Ikeda et al., 2003). This may lead to the opening of the $GABA_A$ receptor channel to allow tonic Cl^- current (Otis et al., 1991; LoTurco et al., 1995). In this situation, $[Cl^-]_i$ should become higher by KCC2 dysfunction (Fig. 3*D*) and functional expression of NKCC1, a Cl^- uptake transporter, in immature facial motoneurons (H. Toyoda and A. Fukuda, unpublished observation). Consequently, neurons become persistently depolarized and cannot produce any action potentials attributable to inactivation of fast sodium channels. In fact, at the time when excess GABA was washed out from the extracellular space by superfusion, the response to VLM stimulation was restored (Fig. 2*B*). Of course, we cannot exclude other possibilities that could ex-

plain the slower transition in the homozygotes than the wild types, for example, difference of the recovery rate of ion gradients. On the other hand, other defects such as poor connection between the rhythm generator neurons, which reside in the parafacial respiratory group (pFRG), and the pattern generator neurons in VLM (H. Onimaru, unpublished observation), might explain the complete lack of spontaneous rhythm generation even after 1 hr superfusion (Fig. 2*B*, right, and data not shown).

What is the inhibitory neural activity observed in the facial nucleus region in wild-type mice?

The presence of inhibitory neuronal activity in the respiratory neurons in E18.5 mice has not been directly demonstrated to date. Rather, it has been reported that the $GABA_A$-mediated response switches from depolarization to hyperpolarization during the first postnatal week (Ritter and Zhang, 2000). However, the present results demonstrated the existence of inhibitory neural activity in the facial nucleus bilaterally in the wild-type E18.5 fetus under adrenaline-stimulated condition (Fig. 3*B*). Furthermore, a fast hyperpolarizing potential was recorded in the ventral respiratory group neurons of neonatal rat (Brockhaus and Ballanyi, 1998). The existence of inhibitory neural activity is consistent with abundant expression of KCC2 in the fetal CNS, including the medulla with preBötC (Hübner et al., 2001; Li et al., 2002). In the standard condition, when the brainstem–spinal cord preparation was perfused with modified Krebs' solution without adrenaline, the respiratory activity recorded in E18.5 wild-type fetuses and newborn mice first appeared in the pFRG (Onimaru and Homma, 2003), similar to newborn rat preparation. The inhibitory neural activity in the facial nucleus region during the inspiratory phase was not detected in the normal respiratory cycle recorded in these preparations (Onimaru, unpublished observation). Therefore, the inhibitory activity induced by adrenaline may represent collateral neural inputs from inspiratory network in the preBötC that was preferentially stimulated by adrenaline.

Similarities of phenotypes between *Atp1a2* knock-out and KCC2 knock-out mice

The KCC2 knock-out mice die immediately after birth as a result of severe motor deficit (Hübner et al., 2001). The absence of spontaneous respiratory rhythm activity was also demonstrated in KCC2 knock-out mice using brainstem–spinal cord preparation, thus resembling the phenotype of *Atp1a2*$^{-/-}$ mice shown in this study. KCC2 also plays a pivotal role in embryonic motoneuron function and spinal cord reflexes (Hübner et al., 2001). Our results also previously showed defective reflex responses such as nociceptive reflex response in *Atp1a2*$^{-/-}$ mice (Ikeda et al., 2003). Other KCC2 knock-out mice in which the KCC2 protein level is reduced to ~5% of the wild type are viable but exhibit frequent and generalized seizures during the first postnatal week and die between postnatal days 10 and 16 (Woo et al., 2002). Interestingly, *Atp1a2*$^{-/-}$ offsprings whose genetic background is the 129Sv strain, show respiratory activity after birth, display frequent and generalized seizures, and die within 24 hr after birth (Ikeda, unpublished observation). The striking phenotypic similarities between mice deficient in the two distinct membrane proteins of KCC2 and Na^+, K^+-ATPase α2 subunit strongly suggests a functional interaction between these proteins in the membrane of neurons.

Functional coupling between Na^+, K^+-ATPase α2 subunit and KCC2

In contrast to the α1 isoform, which maintains generalized cellular homeostasis of Na^+ and K^+ as a housekeeping role, reduction in the α2 subunit has little effect on bulk cytosolic Na^+ concentration (Golovina et al., 2003). The α2 subunit plays more specific roles by colocalization with various ion exchangers (for review, see Lingrel et al., 2003). In the present study, we propose a new model for functional coupling between the Na^+, K^+-ATPase α2 subunit and the neuron-specific K-Cl cotransporter KCC2. Immunoreactivities of KCC2 are found on the plasma membrane of a dendritic shaft, which is thought to be near the excitatory synapse in the rat developing hippocampus (Gulyás et al., 2001). Non-uniform spatial localization of KCC2 within neurons was also observed in the rat adult retina, in which KCC2 is expressed in dendrites but not in cell bodies (Vu et al., 2000). Other studies using electron microscopic immunogold labeling also showed localization of KCC2 in the dendritic plasma membrane of GABAergic neurons close to the inhibitory synapses (Gulácsi et al., 2003). On the other hand, high enrichment of the Na^+, K^+-ATPase α2 subunit was noted in purified synaptic membrane in adult rat brain as well as mouse fetal brain compared with the α1 subunit in neurons (Dolapchieva, 1996; Gorini et al., 2002) (Ikeda, unpublished observations). In the present study, we demonstrated coimmunoprecipitation of the α2 subunit and KCC2 using highly purified synaptic membrane fraction (Fig. 4*D*). Interestingly, the apparent defects in *Atp1a2*$^{-/-}$ fetuses were not observed in all of the regions that expressed the Na^+, K^+-ATPase α2 subunit in the brain but in restricted regions known to highly express KCC2 in the perinatal period, such as amygdala, piriform cortex, and brainstem (Li et al., 2002; Wang et al., 2002). Therefore, it is conceivable that the Na^+, K^+-ATPase α2 isoform and KCC2 are expressed in the same neurons and may colocalize in the synapse. The absence of the α2 subunit would decrease the local intracellular K^+ concentration around KCC2, leading to impairment of KCC2 function, and result in high $[Cl^-]_i$. The excess intracellular Cl^- would switch GABA response to depolarization from hyperpolarization, as shown in the present study (Fig. 3*C*). However, other explanations for the KCC2 dysfunction based on the lack of the membrane α2 subunit are possible (see below).

Ca^{2+} enters the cell through nifedipine-sensitive voltage-gated Ca^{2+} channels triggered by action potential in postsynaptic neuron and reduces KCC2 function in postsynaptic neuron, through a yet unknown pathway (Stell and Mody, 2003; Woodin et al., 2003). High intracellular Ca^{2+} concentrations have been observed in astrocytes and neurons prepared from *Atp1a2*$^{-/-}$ knock-out mice (Golovina et al., 2003; Hartford et al., 2004) (Ikeda, unpublished observations). Thus, it is also possible that KCC2 dysfunction is attributable to high intracellular Ca^{2+} concentration in homozygous neurons and that the Na^+, K^+-ATPase α2 subunit plays a key role in specificity of neural plasticity together with intracellular Ca^{2+} storage site. This possibility should be examined in the future.

References

Abe Y, Furukawa K, Itoyama Y, Akaike N (1994) Glycine response in acutely dissociated ventromedial hypothalamic neuron of the rat: new approach with gramicidin perforated patch-clamp technique. J Neurophysiol 72:1530–1537.

Ballanyi K, Onimaru H, Homma I (1999) Respiratory network function in the isolated brainstem-spinal cord of newborn rats. Prog Neurobiol 59:583–634.

Barnard EA, Skolnick P, Olsen RW, Mohler H, Sieghart W, Biggio G, Braestrup C, Bateson AN, Langer SZ (1998) International Union of Pharmacology. XV. Subtypes of γ-aminobutyric $acid_A$ receptors: classification on the basis of subunit structure and receptor function. Pharmacol Rev 50:291–313.

Ben-Ari Y (2002) Excitatory actions of GABA during development: the nature of the nurture. Nat Rev Neurosci 3:728–739.

Blanco G, Koster JC, Sánchez G, Mercer RW (1995) Kinetic properties of the $\alpha 2\beta 1$ and $\alpha 2\beta 2$ isozymes of the Na,K-ATPase. Biochemistry 34:319–325.

Brockhaus J, Ballanyi K (1998) Synaptic inhibition in the isolated respiratory network of neonatal rats. Eur J Neurosci 10:3823–3839.

Dolapchieva S (1996) Developmental changes of K^+-dependent paranitrophenylphosphatase (Na^+-K^+-ATPase) distribution in the synaptic regions in the cerebral cortex of rats. Neurosci Res 24:309–312.

Feldman JL, Mitchell GS, Nattie EE (2003) Breathing: rhythmicity, plasticity, chemosensitivity. Annu Rev Neurosci 26:239–266.

Golovina VA, Song H, James PF, Lingrel JB, Blaustein MP (2003) Na^+ pump α_2-subunit expression modulates Ca^{2+} signaling. Am J Physiol 284:C475–C486.

Gorini A, Canosi U, Devecchi E, Geroldi D, Villa RF (2002) ATPases enzyme activities during ageing in different types of somatic and synaptic plasma membranes from rat frontal cerebral cortex. Prog Neuropsychopharmacol Biol Psychiatry 26:81–90.

Gray PA, Janczewski WA, Mellen N, McCrimmon DR, Feldman JL (2001) Normal breathing requires preBötzinger complex neurokinin-1 receptor-expressing neurons. Nat Neurosci 4:927–930.

Gulácsi A, Lee CR, Sík A, Viitanen T, Kaila K, Tepper JM, Freund TF (2003) Cell type-specific differences in chloride-regulatory mechanisms and $GABA_A$ receptor-mediated inhibition in rat substantia nigra. J Neurosci 23:8237–8246.

Gulyás AI, Sík A, Payne JA, Kaila K, Freund TF (2001) The KCl cotransporter, KCC2, is highly expressed in the vicinity of excitatory synapses in the rat hippocampus. Eur J Neurosci 13:2205–2217.

Hartford AK, Messer ML, Moseley AE, Lingrel JB, Delamere NA (2004) Na,K-ATPase $\alpha 2$ inhibition alters calcium responses in optic nerve astrocytes. Glia 45:229–237.

Herrera VLM, Cova T, Sassoon D, Ruiz-Opazo N (1994) Developmental cell-specific regulation of Na^+-K^+-ATPase α_1-, α_2-, and α_3-isoform gene expression. Am J Physiol 266:C1301–C1312.

Hübner CA, Stein V, Hermans-Borgmeyer I, Meyer T, Ballanyi K, Jentsch TJ (2001) Disruption of KCC2 reveals an essential role of K-Cl cotransport already in early synaptic inhibition. Neuron 30:515–524.

Ikeda K, Onaka T, Yamakado M, Nakai J, Ishikawa T, Taketo MM, Kawakami K (2003) Degeneration of the amygdala/piriform cortex and enhanced fear/anxiety behaviors in sodium pump $\alpha 2$ subunit (*Atp1a2*)-deficient mice. J Neurosci 23:4667–4676.

Jewell EA, Lingrel JB (1991) Comparison of the substrate dependence properties of the rat Na,K-ATPase $\alpha 1$, $\alpha 2$, and $\alpha 3$ isoforms expressed in HeLa cells. J Biol Chem 266:16925–16930.

Kaila K (1994) Ionic basis of $GABA_A$ receptor channel function in the nervous system. Prog Neurobiol 42:489–537.

Lencesova L, O'Neill A, Resneck WG, Bloch RJ, Blaustein MP (2004) Plasma membrane-cytoskeleton-endoplasmic reticulum complexes in neurons and astrocytes. J Biol Chem 279:2885–2893.

Li H, Tornberg J, Kaila K, Airaksinen MS, Rivera C (2002) Patterns of cation-chloride cotransporter expression during embryonic rodent CNS development. Eur J Neurosci 16:2358–2370.

Lingrel J, Moseley A, Dostanic I, Cougnon M, He S, James P, Woo A, O'Connor K, Neumann J (2003) Functional roles of the α isoforms of the Na,K-ATPase. Ann NY Acad Sci 986:354–359.

LoTurco JJ, Owens DF, Heath MJS, Davis MBE, Kriegstein AR (1995) GABA and glutamate depolarize cortical progenitor cells and inhibit DNA synthesis. Neuron 15:1287–1298.

Moseley AE, Lieske SP, Wetzel RK, James PF, He S, Shelly DA, Paul RJ, Boivin GP, Witte DP, Ramirez JM, Sweadner KJ, Lingrel JB (2003) The Na,K-ATPase $\alpha 2$ isoform is expressed in neurons, and its absence disrupts neuronal activity in newborn mice. J Biol Chem 278:5317–5324.

Nabekura J, Ueno T, Okabe A, Furuta A, Iwaki T, Shimizu-Okabe C, Fukuda A, Akaike N (2002) Reduction of KCC2 expression and $GABA_A$ receptor-mediated excitation after *in vivo* axonal injury. J Neurosci 22:4412–4417.

Onimaru H, Homma I (2003) A novel functional neuron group for respiratory rhythm generation in the ventral medulla. J Neurosci 23:1478–1486.

Otis TS, Staley KJ, Mody I (1991) Perpetual inhibitory activity in mammalian brain slices generated by spontaneous GABA release. Brain Res 545:142–150.

Owens DF, Kriegstein AR (2002) Is there more to GABA than synaptic inhibition? Nat Rev Neurosci 3:715–727.

Payne JA (1997) Functional characterization of the neuronal-specific K-Cl cotransporter: implications for $[K^+]_o$ regulation. Am J Physiol 273:C1516–C1525.

Payne JA, Stevenson TJ, Donaldson LF (1996) Molecular characterization of a putative K-Cl cotransporter in rat brain. A neuronal-specific isoform. J Biol Chem 271:16245–16252.

Payne JA, Rivera C, Voipio J, Kaila K (2003) Cation-chloride co-tansporters in neuronal communication, development and trauma. Trends Neurosci 26:199–206.

Peng L, Martin-Vasallo P, Sweadner KJ (1997) Isoforms of Na,K-ATPase α and β subunits in the rat cerebellum and in granule cell cultures. J Neurosci 17:3488–3502.

Richter DW, Spyer KM (2001) Studying rhythmogenesis of breathing: comparison of *in vivo* and *in vitro* models. Trends Neurosci 24:464–472.

Ritter B, Zhang W (2000) Early postnatal maturation of $GABA_A$-mediated inhibition in the brainstem respiratory rhythm-generating network of the mouse. Eur J Neurosci 12:2975–2984.

Rivera C, Voipio J, Payne JA, Ruusuvuori E, Lahtinen H, Lamsa K, Pirvola U, Saarma M, Kaila K (1999) The K^+/Cl^- co-transporter KCC2 renders GABA hyperpolarizing during neuronal maturation. Nature 397:251–255.

Shelly DA, He S, Moseley A, Weber C, Stegemeyer M, Lynch RM, Lingrel J, Paul RJ (2004) Na^+ pump α_2-isoform specifically couples to contractility in vascular smooth muscle: evidence from gene-targeted neonatal mice. Am J Physiol 286:C813–C820.

Shull GE, Greeb J, Lingrel JB (1986) Molecular cloning of three distinct forms of the Na^+,K^+-ATPase α-subunit from rat brain. Biochemistry 25:8125–8132.

Smith JC, Ellenberger HH, Ballanyi K, Richter DW, Feldman JL (1991) Pre-Bötzinger complex: a brainstem region that may generate respiratory rhythm in mammals. Science 254:726–729.

Stein V, Hermans-Borgmeyer I, Jentsch TJ, Hübner CA (2004) Expression of the KCl cotransporter KCC2 parallels neuronal maturation and the emergence of low intracellular chloride. J Comp Neurol 468:57–64.

Stell B, Mody I (2003) A tale of timing and transport. Neuron 39:729–730.

Sweadner KJ (1989) Isozymes of the Na^+/K^+-ATPase. Biochim Biophys Acta 988:185–220.

Sweadner KJ (1992) Overlapping and diverse distribution of Na-K ATPase isozymes in neurons and glia. Can J Physiol Pharmacol 70:S255–S259.

Toyoda H, Ohno K, Yamada J, Ikeda M, Okabe A, Sato K, Hashimoto K, Fukuda A (2003) Induction of NMDA and $GABA_A$ receptor-mediated Ca^{2+} oscillations with KCC2 mRNA downregulation in injured facial motoneurons. J Neurophysiol 89:1353–1362.

Verheugen JAH, Fricker D, Miles R (1999) Noninvasive measurements of the membrane potential and GABAergic action in hippocampal interneurons. J Neurosci 19:2546–2555.

Vu TQ, Payne JA, Copenhagen DR (2000) Localization and developmental expression patterns of the neuronal K-Cl cotransporter (KCC2) in the rat retina. J Neurosci 20:1414–1423.

Wang C, Shimizu-Okabe C, Watanabe K, Okabe A, Matsuzaki H, Ogawa T, Mori N, Fukuda A, Sato K (2002) Developmental changes in KCC1, KCC2, and NKCC1 mRNA expressions in the rat brain. Dev Brain Res 139:59–66.

Williams JR, Sharp JW, Kumari VG, Wilson M, Payne JA (1999) The neuron-specific K-Cl cotransporter, KCC2. Antibody development and initial characterization of the protein. J Biol Chem 274:12656–12664.

Woo N-S, Lu J, England R, McClellan R, Dufour S, Mount DB, Deutch AY, Lovinger DM, Delpire E (2002) Hyperexcitability and epilepsy associated with disruption of the mouse neuronal-specific K-Cl cotransporter gene. Hippocampus 12:258–268.

Woodin MA, Ganguly K, Poo M-M (2003) Coincident pre- and postsynaptic activity modifies GABAergic synapses by postsynaptic changes in Cl^- transporter activity. Neuron 39:807–820.

Yamada J, Okabe A, Toyoda H, Kilb W, Luhmann HJ, Fukuda A (2004) Cl^- uptake promoting depolarizing GABA actions in immature rat neocortical neurones is mediated by NKCC1. J Physiol (Lond) 557:829–841.